Improved neuron culture using scaffolds made of three-dimensional PDMS micro-lattices

Biomedical Materials

Improved neuron culture using scaffolds made of three-dimensional PDMS micro-lattices

To cite this article before publication: Sisi Li *et al* 2018 *Biomed. Mater.* in press https://doi.org/10.1088/1748-605X/aaa777

Improved neuron culture using three-dimensional PDMS micro-lattices

Sisi Li[ab‡], Francesco Paolo Ulloa Severino[c‡], Jelena Ben[c], Li Wang[ab] , Giulietta Pinato[c], Vincent Torre[c] and Yong Chen[ab*]

[a]*PASTEUR, Département de chimie, École normale supérieure, UPMC Univ. Paris 06, CNRS, PSL Research University, 75005 Paris, France*

[b]*Sorbonne Universités, UPMC Univ. Paris 06, École normale supérieure, CNRS, PASTEUR, 75005 Paris, France*

[c]*Neurobiology Sector, International School for Advanced Studies (SISSA), via Bonomea, 265, 34136 Trieste, Italy*

[‡]*These authors contributed equally to this work*

Abstract: Tissue engineering strives to create functional components of organs with different cell types *in vitro*. One of the challenges is to fabricate scaffolds for three-dimensional (3D) cell culture under physiological conditions. Of particular interesting is to investigate the morphology and function of the central nervous system (CNS) cultured using such scaffolds. Here, we used an elastomer, polydimethylsiloxane (PDMS), to produce lattice-type scaffolds from a photolithography defined template. The photomask with antidot arrays was spin-coated by a thick layer of resist and downward mounted on a rotating stage at angle of 45 °. After exposure for three or more times keeping the same exposure plan but rotated by the same angle, the photoresist was developed to produce a 3D porous template. Afterward, a pre-polymer mixture of PDMS was poured in and cured, followed by a resist etch, resulting in lattice-type PDMS features. Before cell culture, the PDMS lattices were surface functionalized. Culture test has been done using NIH-3T3 cells and primary hippocampal cells from rats, showing homogenously cell infiltration and 3D attachment. As expected, a much higher cell number was found in 3D PDMS lattices than in 2D culture. We also found a higher neuron to astrocyte ratio and a higher degree of cell ramification in 3D culture compared to 2D culture, due to the change of scaffold topography and the elastic properties of the PDMS micro-lattices. Our results demonstrate that the 3D PDMS micro-lattices improve the survival and growth of cells as well as the network formation of neurons. We believe that such an enabling technology is useful for research and clinical applications including disease modeling, regenerative

* Corresponding author. Ecole Normale Supérieure, 24 rue Lhomond, 75231 Paris, France. Tel.: +33 1 44322421; Fax: +33 1 44322402. E-mail address: yong.chen@ens.fr (Y. Chen).

medicine, and drug discovery/drug cytotoxicity studies.

***Keywords**:* Biofabrication, Scaffold, PDMS lattice, Cell culture

1. Introduction

Cell adhesion, migration, proliferation and differentiation are guided by topographic and biochemical cues, which can now be engineered *in vitro* by sophisticated technologies [1]. The previous studies, however, were mostly devoted to the two-dimensional (2D) patterns using photolithography, soft-lithography, nanoimprint lithography and similar techniques [2-4]. Alternatively, non-lithographic techniques such as electrospinning, solvent casting, particulate leaching, etc. have been used to produce stochastic scaffolds [5-7]. More recently, 3D plotting [8-11], fused deposition molding [12, 13], stereo-lithography [14-16], self-propagating photopolymer waveguide processing [17-20], etc., are emerged as rapid prototyping techniques. These techniques are promising but generally of low resolution [21], time-consuming [22], or not biocompatibility for advanced cell assays [23].

In this work, we fabricated well-defined and elastomeric three-dimensional (3D) micro-lattices as scaffolds for neuron culture and neural network formation. Polydimethylsiloxane (PDMS), a widely used elastomer for casting and microfluidic device making, has been chosen because of its non-toxic and easy-processing properties [24-26]. In addition, the Young's module of PDMS is relatively low (0.4 - 4 MPa) and it can be regulated by changing the ratio between catalytic and basic components [27, 28]. Furthermore, the effective Young's module of the substrates made of PDMS micropillars or micro-tripods can be adjusted to match the tissue stiffness (e.g. <1KPa for brain slices) [29]. Besides, PDMS shows high optical transparency throughout the ultraviolet and visible wavelengths [30], which makes it an ideal material for 3D observation of cell behaviors in 3D scaffold in *in vitro*. The fabrication of 3D PDMS scaffolds by layer-by-layer construction has already been reported, showing the relevance of the scaffolds for culture studies [31]. Finally, it has been demonstrated that the micropatterned structures made of PDMS, pre-seeded with neurons, can be used to repair primary motor (M1) cortex lesion which induced a strong motor deficit [32]. Here, we fabricated lattice-type 3D PDMS structures using conventional photolithography and soft-lithography techniques. The conventional photolithography is used to produce 3D templates in a thick layer of resist by backside exposure with an UV light at defined incident angles. Soft lithography is used to cast PDMS into the resist templates, resulting in lattice-type PDMS features after the resist etching. The lattice parameters, i.e. thickness, indication angle and node-to-node space of the lattice units, are adjustable to produce symmetrical and asymmetrical 3D features. The PDMS replica with different geometry parameters are then used to culture NIH-3T3 cell line and primary hippocampal neuron cells of rats. The aim of this work is to fabricate a 3D cell culture platform for

applications in basic research and biomedical engineering. By using conventional lithography techniques, 3D PDMS micro-lattices of different geometry could be produced and our results showed improved survival and formation of neuron networks under optimal culture conditions, thus allowing us to envisage *in vitro* 3D brain models and to overcome the barriers to the central nervous system regeneration. The possibility to peel off the 3D structure of PDMS will further open a route for the applications of the device for *in vivo* studies.

2. Experimental methods

Chemicals and materials: AZ40XT photoresist and AZ developer 726MIF developer were purchased from MicroChemicals GmbH. Chrome photoplates coated with AZ1518 photoresist @ 5300 Å thickness were from Nanofilm Inc, USA. PDMS (RTV615 Kit) was from Momentive. Fibronectin (FN) was from Biopur AG. Dulbecco's minimum essential medium (DMEM), L-glutamine, penicillin/streptomycin (P/S), 0.05% Trypsin-EDTA, Dulbecco's modified phosphate-buffered saline (DPBS), PBS tablets, minimum essential medium (MEM), fetal bovine serum (FBS), gentamycin, goat anti mouse immunoglobulin (Ig) G1 Alexa Fluor® 488, goat anti-mouse IgG2a Alexa Fluor® 594, Fluo4-AM and Pluronic F-127 20% solution in DMSO were purchased from Life Technologies. Rhodamine B, fungizone, paraformaldehyde (PFA), Triton-X-100 (TX), bovine serum albumin (BSA), sodium azide, 4,6-diamidino-2-phenylindole (DAPI), Hoechst 33342, fluorescein isothiocyanate (FITC)-labelled Phalloidin, poly-L-ornithin, D-glucose, Hepes, apo-transferrin, insulin, D-biotin, vitamin B12, cytosine-β-D-arabinofuranoside (Ara-C), glial fibrillary acidic protein (GFAP) and Dimethyl sulfoxide (DMSO) anhydrous, were all purchased from Sigma-Aldrich, Matrigel was purchased from Corning, anti-β-tubulin III (TUJ1) antibodies were purchased from Covance.

Fabrication of 3D templates: The photolithography process was described in **Fig. 1a**. A homemade rotating stage was fixed under collimated UV light with a 45° angle of inclination (**Fig. 1b**). A dot array was created on the positive photoresist on the chrome photoplate using a micro pattern generator (μPG 101, Heidelberg, Germany). After UV exposure, the plate was developed in photoresist developer. The photoresist of exposed dot area was dissolved and then the exposed chrome dot array was etched in chrome etchant. The rest photoresist was removed with acetone. Then, the chrome mask with antidot array is ready to use in the following 3D lattice mould fabrication. AZ40XT photoresist was spin-coated on the chrome mask at a speed

of 1800 rpm for 20 s to reach a thickness of approximately 40 μm. After baking on a hot plate at 126 ℃ for 7 min, it was mounted on the rotation stage with the photoresist downward for backside UV exposure. Each exposure was performed for 90 s with a UV beam at 365 nm (9.2 mW/cm^2). The stage was rotated after each exposure along the major axis of the mask surface to have an equal incident angle. After soft baking at 105 ℃ for 2 min, the resist was developed in AZ726MIF developer for 2 min and rinsed with deionized (DI) water, resulting in a 3D porous template as shown in the inserted SEM image of **Fig. 1c.**

Pattern transfer: A pre-polymer of PDMS mixture at 1:5 ratio was poured on the porous template and degassed in vacuum to remove the bubbles. After solidification at 80 ℃ for 2 h, the AZ resist was dissolved in acetone with ultrasonic (80 mW, 20 min). PDMS layer was then separated from the Cr mask, resulting in a 3D truss structures adhered to the bottom substrate (**Fig.1d**).

SEM imaging: The fabricated AZ templates, the PDMS replica and the PDMS replica with cells were sputter-coated (Quorum technologies Sputter K675XD) with 5 nm gold and observed under a scanning electron microscope (Hitachi S-800) operated at 10 kV.

NIH-3T3 cell culture: The 3D PDMS lattice was sterilized with autoclave at 120 ℃ for 30 min. After drying in an oven at 120 ℃ for 2 h, it was treated with plasma (Plasma Cleaner, Harrick) for 3 min and incubated in 50 μg/ml fibronectin in DPBS at room temperature for 30 min. NIH-3T3 cells were prepared in a culture flask in 37 ℃ incubator with 5% CO_2. The culture medium is DMEM consisting 10% FBS, 1% L-glutamine, 0.1% P/S and 0.01% fungizone. After dissociation in a 0.05% Trypsin-EDTA solution and centrifugation, cells were seeded on the surface of PDMS lattice at a density of 1×10^4 cells/cm^2.

Hippocampal neuron culture: Hippocampal neurons from Wistar rats (P2-P3) were prepared in accordance with the guidelines of the Italian Animal Welfare Act, and their use was approved by the Local Veterinary Service, the SISSA Ethics Committee board and the National Ministry of Health (Permit Number: 630-III/14) in accordance with the European Union guidelines for animal care (d.1.116/92; 86/609/C.E.). The animals were anaesthetized with CO_2 and sacrificed by decapitation, and all efforts were made to minimize suffering. The dissection procedure for the hippocampus isolation were done as suggested elsewhere [33] and then modified as described below.

All substrates (2D glass coverslips, 2D PDMS and 3D PDMS) were treated with air plasma-cleaner in order to facilitate cell adhesion and at the end sterilized with an UV lamp. Soon after the

substrates were coated with 50 μg/ml poly-L-ornithin overnight and coated with Matrigel just before cells seeding. Dissociated cells from isolated hippocampus were plated at a concentration of 6×10^5 cells/ml on each substrate in Neural Medium (MEM with GlutaMAXTM supplemented with 10% FBS, 0.6% D-glucose, 15 mM Hepes, 0.1 mg/ml apo-transferrin, 30 μg/ml insulin, 0.1 μg/ml D-biotin, 1 μM vitamin B12, and 2.5 μg/ml gentamycin). After 48 hours, 2 μM Ara-C was added to the culture medium to block glial cell proliferation, and the concentration of FBS was decreased to 5%. Half of the medium was changed every 2–3 days. The neuronal cultures were maintained in an incubator at 37 ℃, 5% CO_2 and 95% relative humidity.

Confocal imaging of PDMS lattice and NIH-3T3 cells: Before cell loading, the PDMS lattice was treated with plasma for 3 min and immerged in 100 mM Rhodamine B in DI water for overnight. NIH-3T3 cells were fixed in 4% PFA for 30 min and then permeabilized in PBS containing 0.5% TX for 30 min. After blocked in blocking buffer (0.1% TX, 3% BSA, 0.1% sodium azide in PBS) for 30 min again, cell skeleton and nuclei were stained with 5 μg/mL phalloidin-FITC and 300 nM DAPI in PBS for 30min, respectively. All the procedures were operated at room temperature and there were PBS rinsing three times between each solution change. The samples were imaged under the Carl Zeiss laser scanning microscopes LSM 710.

Morphological and immunocytochemical analysis. Cells were fixed in 4% paraformaldehyde containing 0.15% picric acid in PBS, saturated with 0.1 M glycine, permeabilized with 0.1% Triton X-100, saturated with 0.5% BSA in PBS and then incubated for 1 h with primary antibodies: mouse monoclonal GFAP, anti-β-tubulin III (TUJ1) antibodies. The secondary antibodies were goat anti mouse immunoglobulin (Ig) G1 Alexa Fluor® 488, goat anti-mouse IgG2a Alexa Fluor® 594, and the incubation time was 30 min. Nuclei were stained with 2 μg/ml in PBS Hoechst 33342 for 5 min. All the incubations were performed at room temperature (20–22 ℃). The cells were examined using a Leica DM6000 fluorescent microscope equipped with DIC and fluorescence optics, CCD camera and Volocity 5.4 3D imaging software (PerkinElmer, Coventry, UK). The fluorescence images were collected with a 40X magnification and 0.5 NA objective. Image J by W. Rasband (developed at the U.S. National Institutes of Health and available at http://rsbweb.nih.gov/ij/) was used for image processing.

Calcium Imaging. The cells were incubated with 4 μM of the cell-permeable calcium dye Fluo4-AM, dissolved in DMSO anhydrous, and Pluronic F-127 20% solution in DMSO at a ratio of 1:1 in Neural Medium at 37 °C for 1 hour. After incubation, the cultures were washed for 30 min

with Ringer's solution (145 mM NaCl, 3 mM KCl, 1.5 mM CaCl2, 1 mM MgCl2, 10 mM glucose and 10 mM Hepes, pH 7.4) and then transferred to the stage of a Nikon Eclipse Ti-U inverted microscope, an HBO 103 W/2 mercury short arc lamp (Osram, Munich, Germany), a mirror unit (exciter filter BP 465–495 nm, dichroic 505 nm, emission filter BP 515–555) and an Electron Multiplier CCD Camera C9100-13 (Hamamatsu Photonics, Japan). The experiments were performed at RT, and images were acquired using the NIS Element software (Nikon, Japan) with an S-Fluor 20x/0.75 NA objective at a sampling rate of 5 Hz with a spatial resolution of 256 × 256 pixels for 10–20 min. To avoid saturation of the signals, excitation light intensity was attenuated by ND4 and ND8 neutral density filters (Nikon).

Statistical Analysis. Data are shown as the mean ± s.e.m from at least three neuronal cultures. For the morphological analysis of immunofluorescence images, n refers to the number of images analysed. The number of replicates and statistical tests used for each experiment are mentioned in the respective figure legends or in the Results and discussion section. Significance was set to *$p < 0.05$, **$p < 0.01$ and ***$p < 0.001$.

3. Results and discussion

3.1 Fabrication of PDMS micro-lattices

Contact lithography is commonly used in research laboratories to replicate the 2D patterns by UV exposing a photoresist layer spin coated on a substrate through a photomask in direct contact with the resist. To reach the highest resolution and the best pattern stability, we spun coat a thick resist layer directly on the photomask and then performed the sequential steps with the same substrate until the release of the PDMS replica (**Fig. 1a**). Since all steps are bench process and the photomask can be used for many times, this fabrication technique remains straightforward and low cost.

The SEM image of the PDMS replica in **Fig.1d** shows a 3D lattice feature with tetrahedral-type unit-cell originated from the same aperture, defined by the antidote array on the 2D photomask and the three directional UV exposures. Since the symmetry, the porosity and the interconnectivity may all affect the cell culture performance, we fabricated 3D lattices of PDMS with different geometry parameters.

We firstly studied the pattern geometry by rotating 120 ° or 90 ° the sample stage after each

exposure, resulting in a tripod structure (**Fig. 2a**) or a four-fold symmetry (**Fig. 2b**). Asymmetric unit-cell can also be achieved by changing the rotation angle after each exposure. **Fig. 2c- 3e** show asymmetrical lattice structures by rotating the sample stage three times with angle of 60 °-60 °-240 °, 90 °-90 °-180 °, and 150 °-150 °-60 ° respectively. We also evaluated the fabrication performance by changing the resist thickness and the incident angle of the UV light. **Fig. 3a1** and **a2** show the SEM images of the PDMS lattices obtained with initial resist layer thickness of 40 μm and 25 μm, respectively. **Fig. 3b1** and **b2** show the SEM images of the PDMS lattices obtained with an UV incident angle is 60 ° and 45 ° respectively. As can be seen, the resulted beam angle of the structure is around 35 ° and 28 °, respectively, which are in agreement with the calculation based on Snell' law.

The geometry of the PDMS lattices is primarily determined by the antidot diameter and pitch size of the photomask. By varying the diameter and pitch size of the antidot but keeping the same lattice height (40 μm), we produced 3D PDMS lattices of different geometry. As shown by the SEM images of **Fig. 4a** and **4b** (pitch size 40 μm, diameter 20 μm and 15 μm) and **Fig. 4c and 4d** (pitch size 80 μm, diameter 20 μm and 15 μm), the bigger the diameter, the smaller the node-to-node space. If the pore size is too large, the resulted features look more like 3D pillars (**Fig. 4e**). **Figure 5** shows the PDMS features obtained with triangle arrays of antidots with 4 μm diameter and three different pitch sizes: 15 μm (**Fig. 5a1** and **a2**), 18 μm (**Fig. 5b1** and **b2**) and 24 μm (**Fig. 5c1** and **c2**), respectively. For larger pitch sizes, the lattice feature collapses due to insufficient mechanical strength, as showed in **Fig. 5d**. By changing gradually the lattice spacing in the same mask, we could achieve a 3D gradient lattice as showed in **Fig. 5e**. Finally, the fabricated PDMS structures could be peeled off (**Fig. S1**), making it possible to be used for other purposes such as microfluidic integration.

3.2 Biocompatibility test with NIH-3T3 cell line

We choose 40 μm-height and three-fold symmetric PDMS lattices with 6 μm diameter and 28 μm pitch size (**Fig. 6a**) for cell culture test. Before sterilization, we stained the PDMS lattice with Rhodamine (red) for easy structure observation under laser confocal microscopy. Then, we seeded NIH-3T3 cells on the lattice surface and cultured them for 2 days. Thanks to the optical transparency of PDMS, we clearly observed adhesion and extension of actin filaments along the 3D lattice surface under confocal microscopy (**Fig. 6b and 6c)**. Here, actin filaments and nuclei were respectively stained by FITC (green) and DAPI (blue). From **Fig. 6h-j**, we also observed the actin filaments crossed the free space of the 3D lattice features, which should be more tissue-like for *in vitro* studies.

The 3D embedment of cell nuclei (**Fig. 6d**) and cell cytoskeleton (**Fig. 6e and 6f**) in the 3D micro-lattice of PDMS both provide the evidence of natural cuboidal cell geometry, not like often observed flatten feature in conventional 2D cultures. However, the shape of the nuclei could be deformed by reducing the pitch size of the lattice and this deformation is inversely proportional to the spacing between the lattice features **(Fig. 6g)**. Previously, it has been shown that both stem cell proliferation and differentiation were correlated to the cell shape [34, 35]. The PDMS lattices with defined geometry could be potentially applied in stem cell research.

3.3 Culture of primary hippocampal neurons

Primary hippocampal neurons are commonly used to study 3D network formation on substrates made by different materials [7, 36]. Here, we used hippocampal neurons from rats to co-culture neurons and astrocytes and show the possibility of a 3D neuronal network formation with the help of a PDMS lattice of 15 μm diameter, 80 μm pitch size and ~40 μm heights (**Fig. 6**). Cells were homogeneously distributed on the structure (**Fig. 7a**) and were able to form an interconnected and mature network after 8 days *in vitro* (DIV) (**Fig. 7b**). From the SEM images both glia cells (**Fig. 6c**) and neurons (**Fig. 7d**) showed a three-dimensional morphology characterized by rounder cell body and neurites projected in all the directions. Glia cells show a flat but ramified morphology whereas neurons have thinner processes (**Fig. 7e**) that, once contacted the surface either of other cells or of the PDMS, highly ramify. These details show a good interaction between cells and material that is extremely important in tissue engineering. Moreover, slight bending of the pillars can be observed (**Fig. 7a** and **7b**) due to the cell interaction with the PDMS features. In turn, the cell adhesion forces might be determined [37, 38].

Immunostaining for neuronal and astrocytes markers, TUJ-1 and GFAP respectively (**Fig. 8**), confirmed the observation made from the SEM images. Compared to the standard glass (**SI Fig. S2**) and to the flat 2D PDMS substrates (**Fig. 8a**), on the 3D PDMS substrates (**Fig. 8b**), we can observe a complex morphological ramification of both neurons and astrocytes. Besides, we found a higher cell population density (215 cell/mm^2, 220 cell/mm^2 and 544 cell/mm^2 respectively) on the 3D PDMS lattice, due to the three-dimensionality of the substrates which offer more surfaces for cell adhesion. The increase of the cell density is 3D lattices can also be attributed to improved cellular microenvironment, in consistent with the previous finding for rat primary hippocampal and cortical cultures in PDMS micro channels [39, 40]. On 3D PDMS 51% cells are neurons and 31% are astrocytes, the remained part is not identified cells (e.g. microglia), while only 33.3 % and 40.3 % of

cells are neurons on the Glass and 2D-PDMS respectively.

Clearly, the neuron density in 3D environment is significant higher than that 2D culture but the difference in astrocyte density is less remarkable between 3D and 2D cultures (Glass: 33.3% of neurons, 59.3% of astrocytes; 2D PDMS: 40.3% of neurons, 58.1% of astrocytes) (**Fig 8c**). The calcium activity recordings of growing neurons on 3D PDMS lattice (**Fig. 8d**) show that they are healthy and alive and that the proposed method is reliable for further studies and applications. In particular, this method offers a new platform to reconstruct 3D *in vitro* neuronal network with ramified and *in vivo*-like morphology, thanks to more appropriate topographical cues and elastic properties of the substrate, compared to the bare glass and the flat 2D PDMS. Therefore, we can assess that the 3D-PDMS lattices improve the survival and growth of the neurons and support the neural network formation and maturation. Consequently, improved drug screening and electrophysiological experiments can be expected. Finally, due to the fact that the PDMS lattices can be peeled off from the substrate (**Supp. Fig.2**), it would be interesting to use them in tissue engineering and transplantation assays [32].

4. Conclusion

Here we report a fabrication process of PDMS micro-lattices using backside photolithography at different incident angles and soft lithography for 3D casting. The fabricated 3D lattices were used to evaluate cell culture performance using NIH-3T3 cell line and primary hippocampal neurons of rats. Homogenous cell infiltration and 3D attachment were observed using different optical techniques. Increased cell number and neuron percentage as well as improved cell ramification were found comparing to the 2D culture showing the great potential of the proposed culture system. Since the geometry and the interconnectivity of the PDMS lattice could be precisely tuned, more systematic studies can be developed. The proposed fabrication process is straightforward and simple, which can probably be applied to a number of *in vitro* and *in vivo* studies.

Acknowledgments

This work was supported by European Commission through project contract (Neuroscaffolds) and Agence de Recherche Nationale under contract No. ANR-13-NANO-0011-01 (Pillarcell). We want to thank also Mattia Fanetti for his assistance during the SEM imaging sessions.

References

1. Théry, C., et al., *Isolation and characterization of exosomes from cell culture supernatants and biological fluids.* Current protocols in cell biology, 2006: p. 3.22. 1-3.22. 29.
2. Kidambi, S., et al., *Cell adhesion on polyelectrolyte multilayer coated polydimethylsiloxane surfaces with varying topographies.* Tissue engineering, 2007. **13**(8): p. 2105-2117.
3. Karuri, N.W., et al., *Biological length scale topography enhances cell-substratum adhesion of human corneal epithelial cells.* Journal of cell science, 2004. **117**(15): p. 3153-3164.
4. Li, S., et al., *Fabrication of gelatin nanopatterns for cell culture studies.* Microelectronic Engineering, 2013. **110**: p. 70-74.
5. Shen, F., et al., *A study on the fabrication of porous chitosan/gelatin network scaffold for tissue engineering.* Polymer international, 2000. **49**(12): p. 1596-1599.
6. Sherwood, J.K., et al., *A three-dimensional osteochondral composite scaffold for articular cartilage repair.* Biomaterials, 2002. **23**(24): p. 4739-4751.
7. Tang, Y., et al., *Patch method for culture of primary hippocampal neurons.* Microelectronic Engineering, 2017. **175**: p. 61-66.
8. Landers, R. and R. Mülhaupt, *Desktop manufacturing of complex objects, prototypes and biomedical scaffolds by means of computer‐assisted design combined with computer‐guided 3D plotting of polymers and reactive oligomers.* Macromolecular Materials and Engineering, 2000. **282**(1): p. 17-21.
9. Landers, R., et al., *Fabrication of soft tissue engineering scaffolds by means of rapid prototyping techniques.* Journal of materials science, 2002. **37**(15): p. 3107-3116.
10. Ang, T., et al., *Fabrication of 3D chitosan–hydroxyapatite scaffolds using a robotic dispensing system.* Materials Science and Engineering: C, 2002. **20**(1): p. 35-42.
11. Landers, R., et al., *Rapid prototyping of scaffolds derived from thermoreversible hydrogels and tailored for applications in tissue engineering.* Biomaterials, 2002. **23**(23): p. 4437-4447.
12. Zein, I., et al., *Fused deposition modeling of novel scaffold architectures for tissue engineering applications.* Biomaterials, 2002. **23**(4): p. 1169-1185.
13. Hutmacher, D.W., et al., *Mechanical properties and cell cultural response of polycaprolactone scaffolds designed and fabricated via fused deposition modeling.* Journal of biomedical materials research, 2001. **55**(2): p. 203-216.
14. Bertsch, A., H. Lorenz, and P. Renaud, *3D microfabrication by combining microstereolithography and thick resist UV lithography.* Sensors and Actuators A: Physical, 1999. **73**(1): p. 14-23.
15. Melchels, F.P., et al., *Mathematically defined tissue engineering scaffold architectures prepared by stereolithography.* Biomaterials, 2010. **31**(27): p. 6909-6916.
16. Lee, K.-W., et al., *Poly (propylene fumarate) bone tissue engineering scaffold fabrication using stereolithography: effects of resin formulations and laser parameters.* Biomacromolecules, 2007. **8**(4): p. 1077-1084.
17. Schaedler, T.A., et al., *Ultralight metallic microlattices.* Science, 2011. **334**(6058): p. 962-965.
18. Kisailus, D., A.J. Jacobsen, and C. Zhou, *Three-dimensional biological scaffold and method*

of making the same. 2013, Google Patents.
19. Jacobsen, A.J., *Optically oriented three-dimensional polymer microstructures*. 2008, Google Patents.
20. Kisailus, D., A.J. Jacobsen, and C. Zhou, *Three-dimensional biological scaffold compromising polymer waveguides*. 2012, Google Patents.
21. Zhang, B., et al., *3D printing of high-resolution PLA-based structures by hybrid electrohydrodynamic and fused deposition modeling techniques.* Journal of Micromechanics and Microengineering, 2016. **26**(2): p. 025015.
22. Bassoli, E., et al., *3D printing technique applied to rapid casting.* Rapid Prototyping Journal, 2007. **13**(3): p. 148-155.
23. Renbutsu, E., et al., *Preparation and biocompatibility of novel UV-curable chitosan derivatives.* Biomacromolecules, 2005. **6**(5): p. 2385-2388.
24. Kane, R.S., et al., *Patterning proteins and cells using soft lithography.* Biomaterials, 1999. **20**(23): p. 2363-2376.
25. Singhvi, R., et al., *Engineering cell shape and function.* Science, 1994. **264**(5159): p. 696-698.
26. Takayama, S., et al., *Patterning cells and their environments using multiple laminar fluid flows in capillary networks.* Proceedings of the National Academy of Sciences, 1999. **96**(10): p. 5545-5548.
27. Wang, Z., A.A. Volinsky, and N.D. Gallant, *Crosslinking effect on polydimethylsiloxane elastic modulus measured by custom‐built compression instrument.* Journal of Applied Polymer Science, 2014. **131**(22).
28. Johnston, I., et al., *Mechanical characterization of bulk Sylgard 184 for microfluidics and microengineering.* Journal of Micromechanics and Microengineering, 2014. **24**(3): p. 035017.
29. Migliorini, E., et al., *Acceleration of neuronal precursors differentiation induced by substrate nanotopography.* Biotechnology and bioengineering, 2011. **108**(11): p. 2736-2746.
30. Yoon, Y., D.-W. Lee, and J.-B. Lee, *Fabrication of optically transparent PDMS artificial lotus leaf film using underexposed and underbaked photoresist mold.* Journal of Microelectromechanical Systems, 2013. **22**(5): p. 1073-1080.
31. Mata, A., et al., *A three-dimensional scaffold with precise micro-architecture and surface micro-textures.* Biomaterials, 2009. **30**(27): p. 4610-4617.
32. Vaysse, L., et al., *Micropatterned bioimplant with guided neuronal cells to promote tissue reconstruction and improve functional recovery after primary motor cortex insult.* Biomaterials, 2015. **58**: p. 46-53.
33. Beaudoin III, G.M., et al., *Culturing pyramidal neurons from the early postnatal mouse hippocampus and cortex.* Nature protocols, 2012. **7**(9): p. 1741-1754.
34. Kumar, G., et al., *The determination of stem cell fate by 3D scaffold structures through the control of cell shape.* Biomaterials, 2011. **32**(35): p. 9188-9196.
35. Kumar, G., et al., *Freeform fabricated scaffolds with roughened struts that enhance both stem cell proliferation and differentiation by controlling cell shape.* Biomaterials, 2012. **33**(16): p. 4022-4030.
36. Severino, F.P.U., et al., *The role of dimensionality in neuronal network dynamics.* Scientific Reports, 2016. **6**.

37. Li, J., et al., *Culture substrates made of elastomeric micro-tripod arrays for long-term expansion of human pluripotent stem cells.* Journal of Materials Chemistry B, 2017. **5**(2): p. 236-244.
38. Fu, J., et al., *Mechanical regulation of cell function with geometrically modulated elastomeric substrates.* Nature methods, 2010. **7**(9): p. 733-736.
39. Habibey, R., et al., *A microchannel device tailored to laser axotomy and long-term microelectrode array electrophysiology of functional regeneration.* Lab on a Chip, 2015. **15**(24): p. 4578-4590.
40. Habibey, R., et al., *A multielectrode array microchannel platform reveals both transient and slow changes in axonal conduction velocity.* Scientific reports, 2017. **7**: p. 8558.

Figure caption

Figure 1 Fabrication of the PDMS 3D lattice. (a) The fabrication process flow; (b) Backside UV exposure at incident angles; (c) SEM top view of the fabricated AZ40XT 3D template and; (d) SEM side view of the replicated PDMS 3D lattices. The diameter of antidots on Cr mask is 4 μm diameter and the period is 18 μm. Scale bar is 10 μm.

Figure 2 SEM images of symmetrical and asymmetrical PDMS 3D lattices. (a) 3-fold symmetry; (b) 4-fold symmetry; Asymmetry with three side vertex angles: (c) 60°-60°-240°; (d) 90°-90°-180°; (e) 150°-150°-60°. Scale bar is 10 μm.

Figure 3 SEM images of PDMS 3D lattices obtained with initial resist layer thickness of 40 μm (a1) and 25μm (a2) and member incident angles of 35° (b1) and 28° (b2), respectively. Scale bar is 10 μm.

Figure 4 SEM images of PDMS 3D lattices with different diameter resulted from different pore size. (a) 20 μm diameter, 40 μm pitch size; (b) 15 μm diameter, 40 μm pitch size;(c) 20 μm diameter, 80 μm pitch size; (d) 15 μm diameter, 80 μm pitch size (e) 30 μm diameter, 80 μm pitch size. Scale bar: 100um

Figure 5 SEM images of PDMS 3D lattices with 4 μm diameter but different pitch sizes: (a) 15 μm; (b) 18 μm; (c) 24 μm; (d) 28 μm. (e) pitch size changing from 12.5 μm to 18.5 μm. (a1), (b1), (c1), (d) and (e) are top view images. (a2), (b2) and (c2) are side view images. Scale bar is 10 μm.

Figure 6 NIH-3T3 cells in PDMS 3D lattices after culture for 2 days. (a) 3D view of a confocal Z-stack of PDMS lattice of 6 μm diameter, 28 μm pitch size and 40 μm height. (b) 3D view of a confocal Z-stack of cell actin filaments adhered on the lattice surface. (c) Merged image of (a) and (b). (d) 3D view of a confocal Z-stack of cell nuclei trapped in the PDMS lattice of (a). (e) Enlarged image of (d) but rotated in 3D space to clearly show the cell nuclei 3D distribution in the PDMS lattice. (f) Nuclei shape of the cells in (e). (g) Z-slice of cells in the PDMS lattice of 4 μm diameter, 14 μm pitch size and 40 μm height. (h) Z-slice of cells in the PDMS lattice of (a). (i)(j) SEM images of actin filaments crossing the free space of the PDMS lattice.

Figure 7 Primary hippocampal neuron culture in PDMS 3D lattices: (a-b) SEM images hippocampal co-culture after 8 DIV. (c-f) Enlarged view of the SEM images showing glia cell (g) and neuron (n) as well as the dendritic arborization and neural attachment on the PDMS surface (e,f).

Figure 8 Morphological differences among 2D (a) and 3D (b) PDMS substrates. One way ANOVA assuming normal distribution was performed to determine whether there was a significant differences between the glass (n=4), 2D-PDMS (n=3), 3D-PDMS (n=4) with respect to the number of neurons and astrocytes (c) for mm^2 after 8 DIV. (2D-PDMS vs 3D-PDMS $p<0,001$; Glass vs 3D-PDMS $p<0,001$). Example traces of calcium activity from neurons growth on 3D PDMS lattice (d).

Figure1

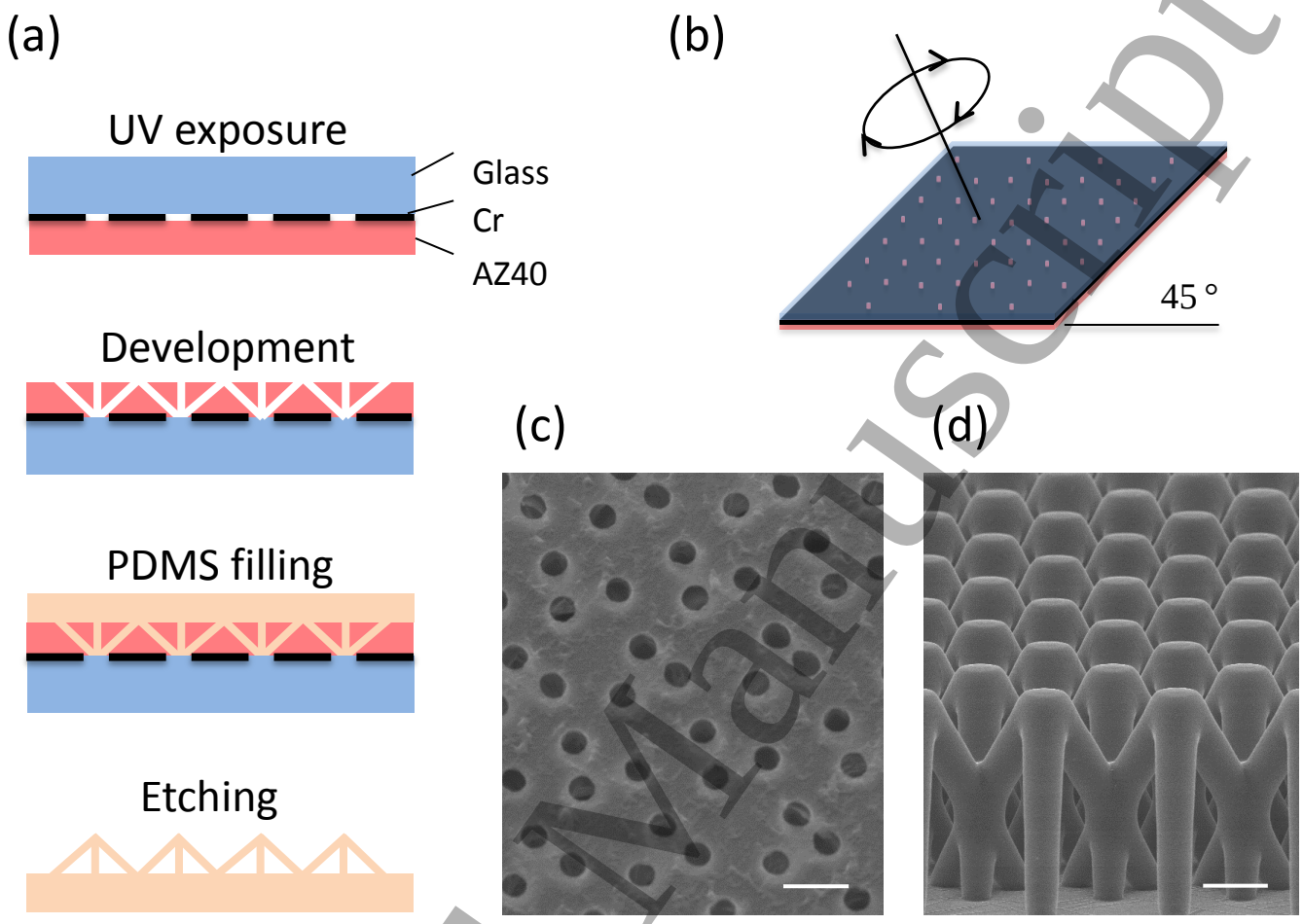

Figure 2

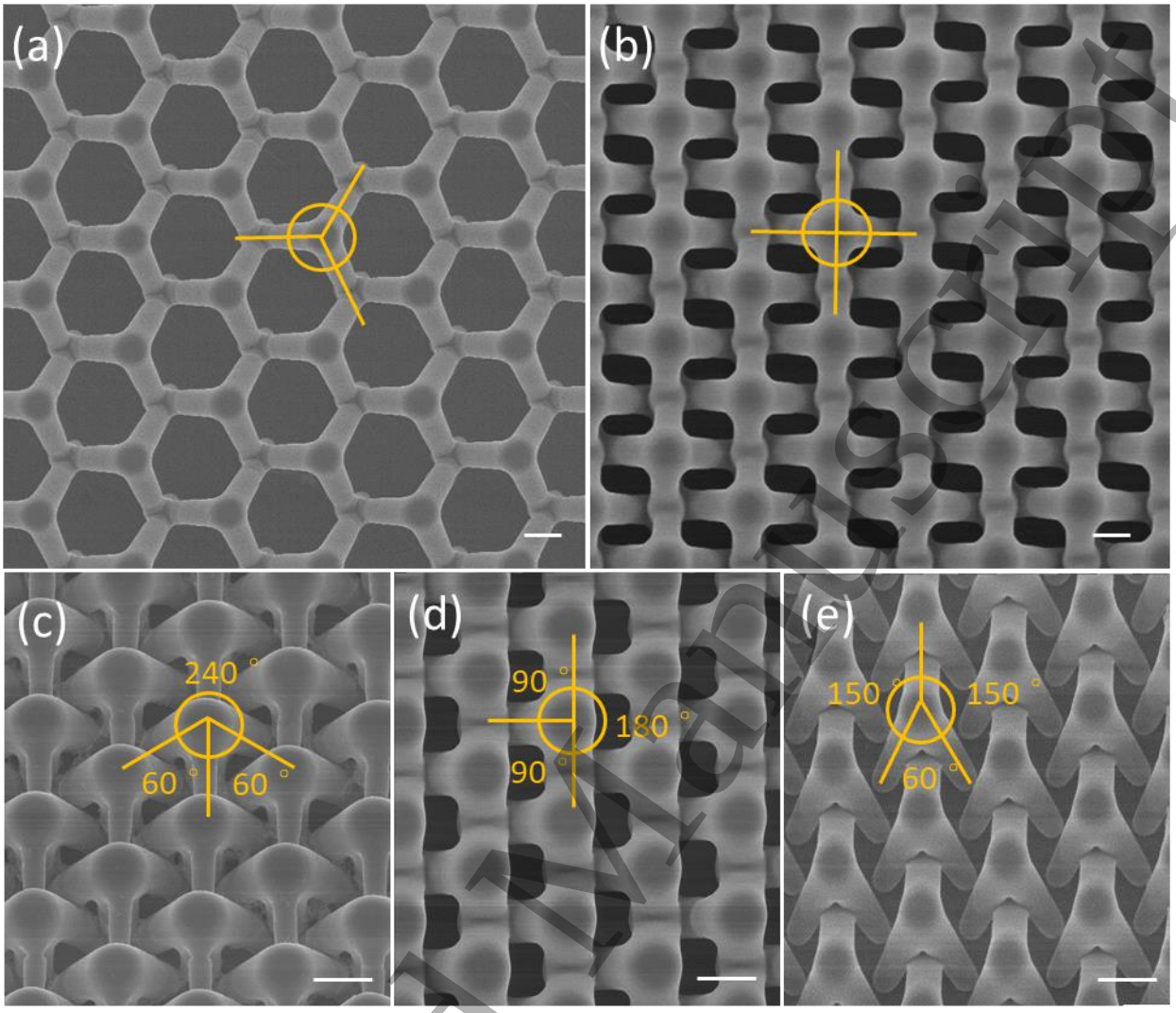

Figure 3

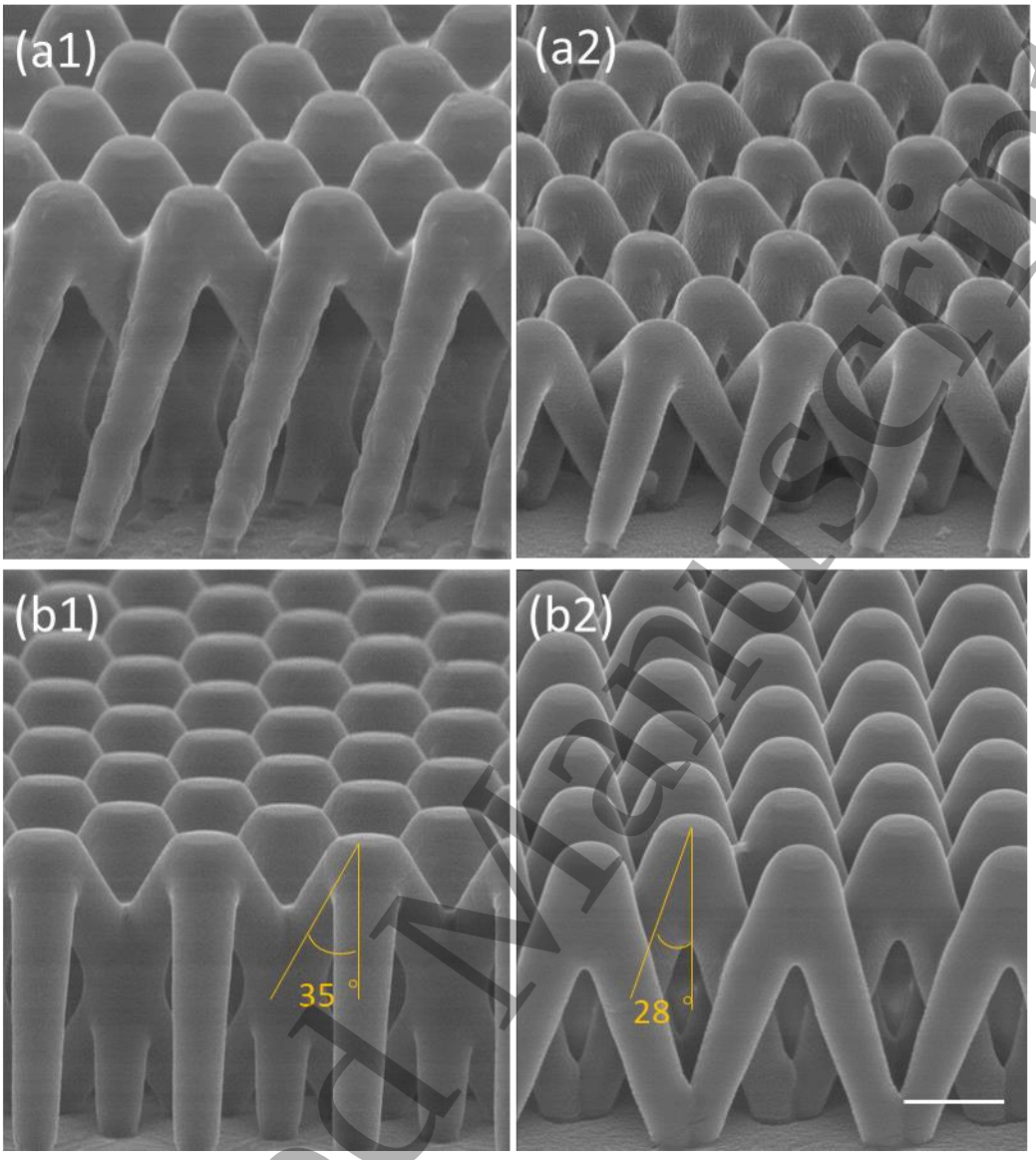

Figure 4

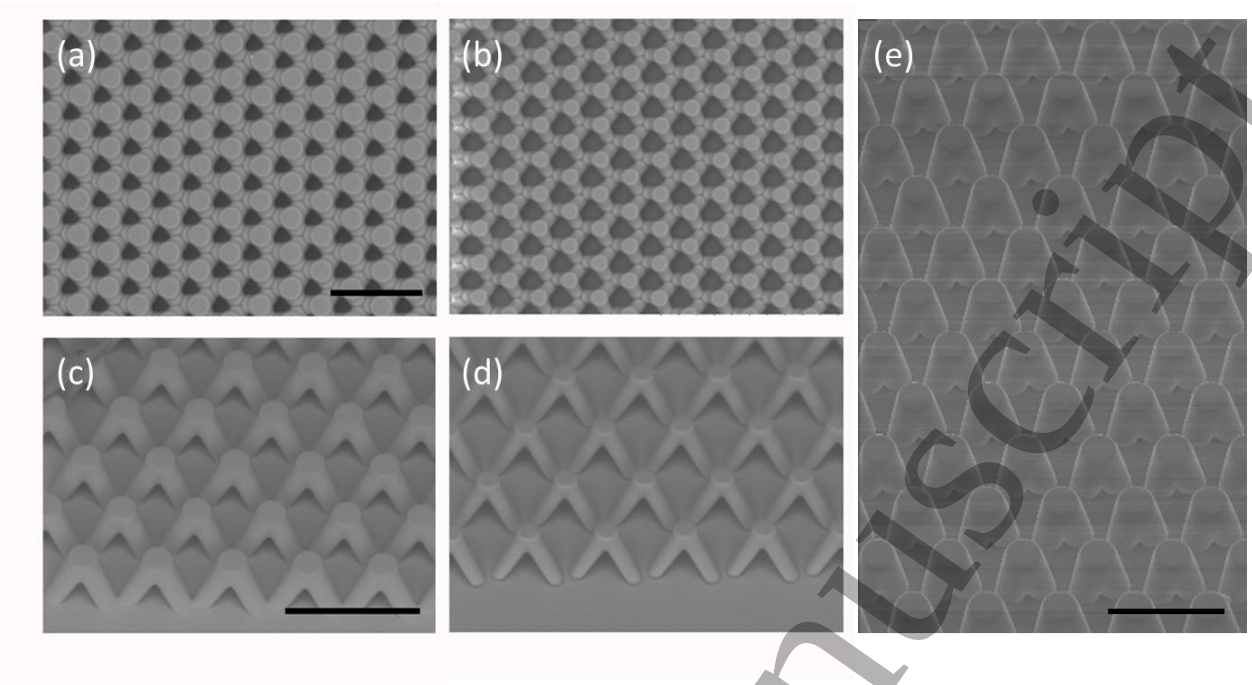

Figure 5

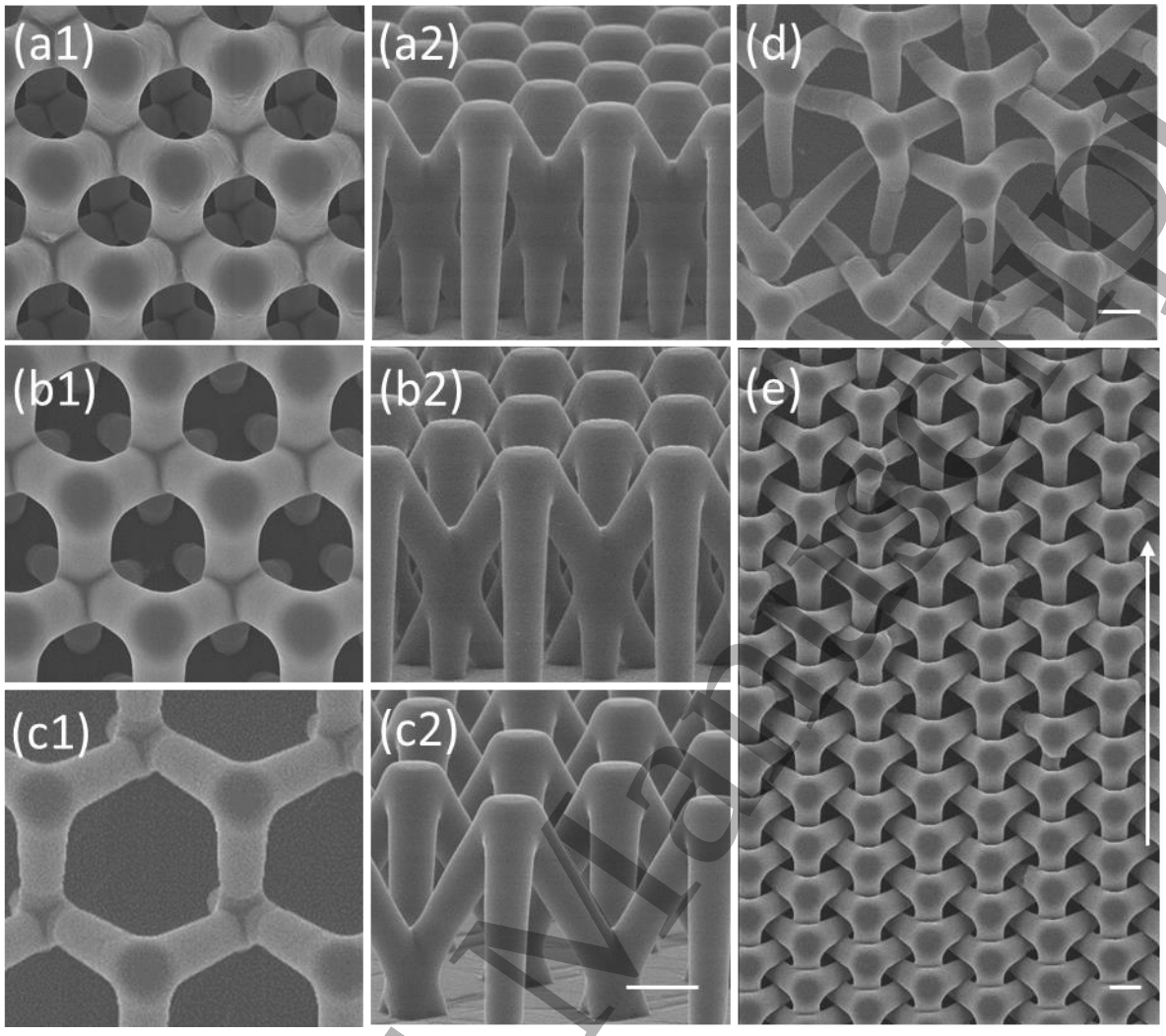

Figure 6

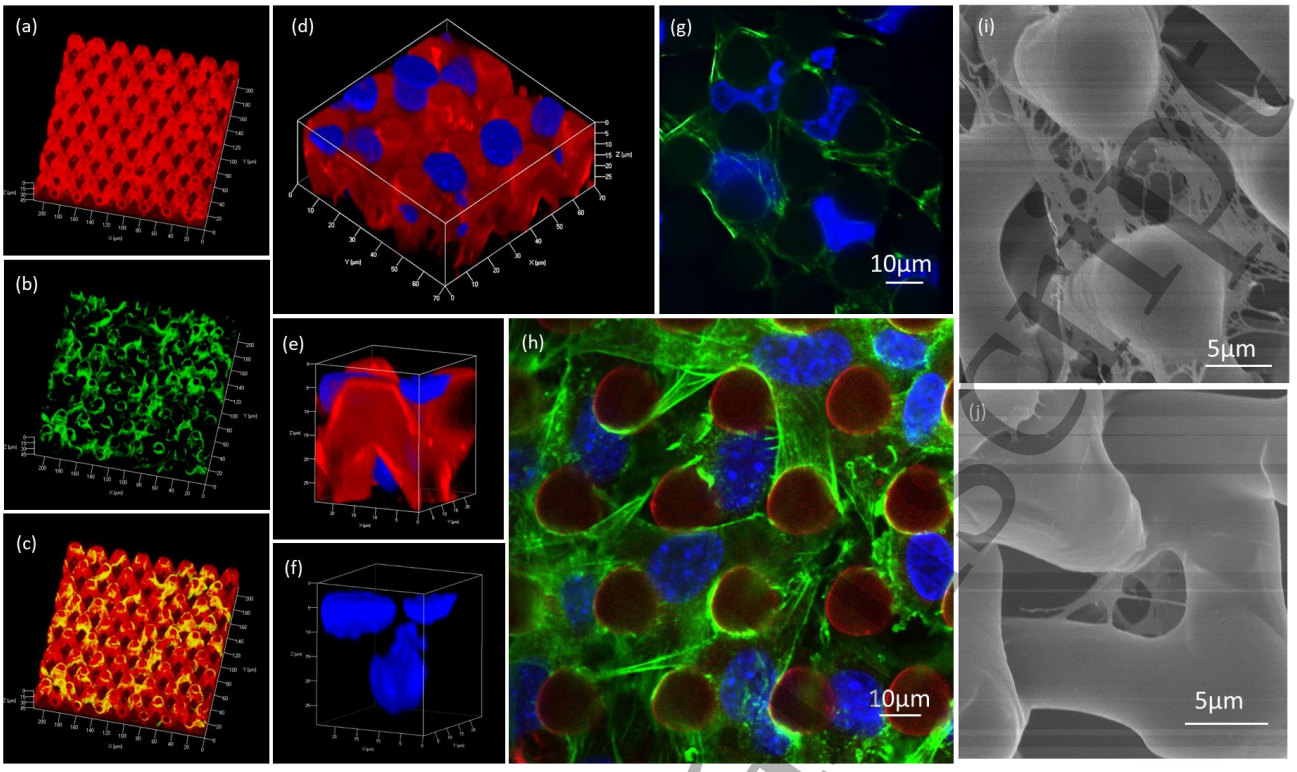

Figure 7

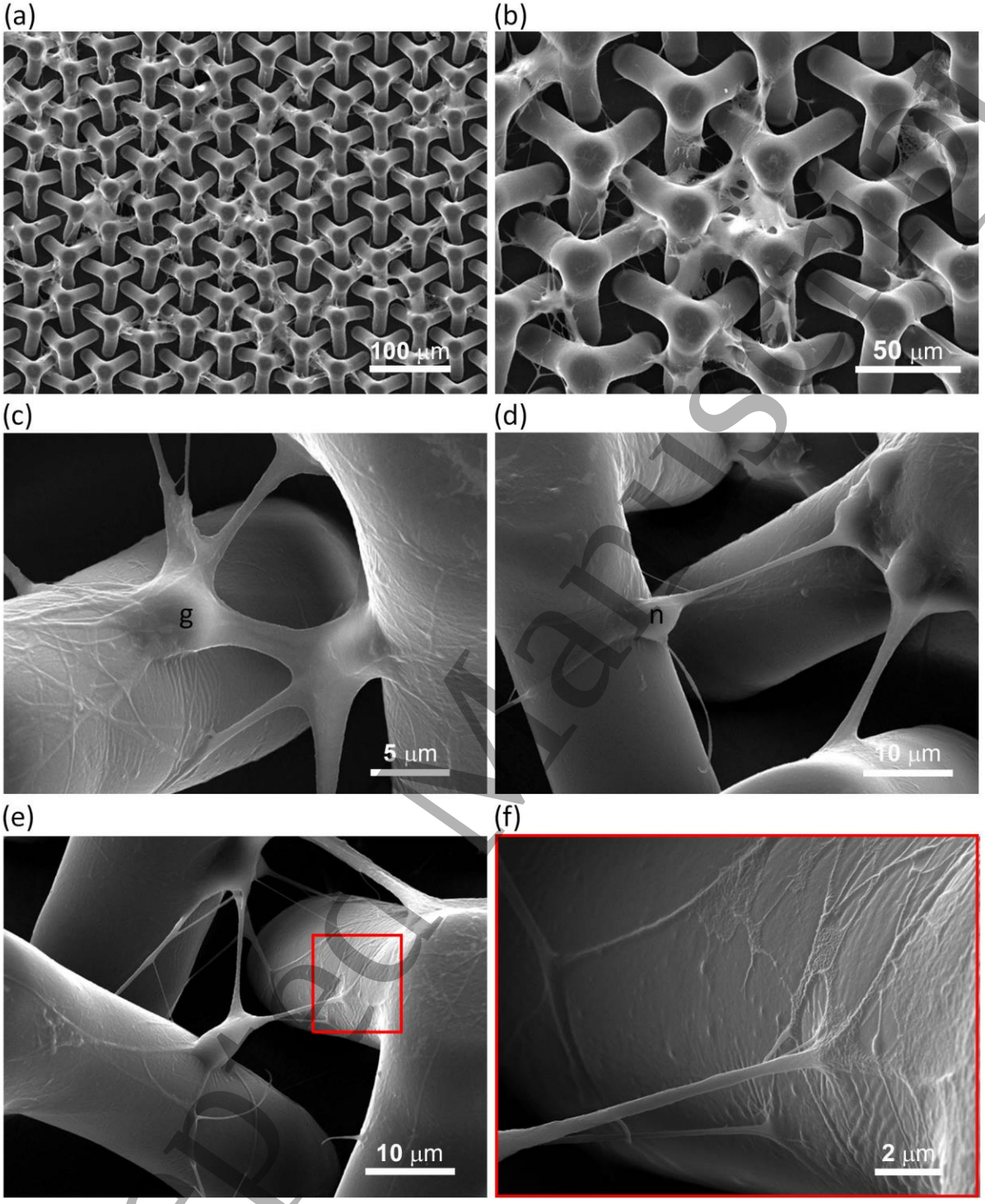

Figure 8